Acta Crystallographica Section D
Biological Crystallography
ISSN 0907-4449

X-ray structure of nitric oxide reductase (cytochrome P450nor) at atomic resolution

Hideaki Shimizu,† Sam-Yong Park,‡ Yoshitsugu Shiro and Shin-ichi Adachi*

RIKEN Harima Institute/SPring-8, 1-1-1 Kouto, Mikazuki, Sayo, Hyogo 679-5148, Japan

† Present address: Department of Molecular Biology and Biochemistry, University of California Irvine, CA 92697-3900, USA.
‡ Present address: Division of Protein Design, Graduate School of Integrated Science, Yokohama City University, 1-7-29 Suehiro, Tsurumi, Yokohama, 230-0045, Japan.

Correspondence e-mail: sadachi@spring8.or.jp

Received 16 July 2001
Accepted 15 October 2001

PDB References: cytochrome P450nor (ferric form), 1jfb; cytochrome P450nor (ferrous CO form), 1jfc.

Crystal structures of the nitric oxide reductase cytochrome P450nor (P450nor) in the ferric resting and the ferrous carbonmonoxy (CO) states have been determined at 1.00 and 1.05 Å resolution, respectively. P450nor consists of 403 amino-acid residues (46 kDa) and is one of the largest proteins refined to this resolution so far. The final models have conventional R factors of 10.2% (ferric resting) and 11.7% (ferrous CO), with mean coordinate errors of 0.028 (ferric resting) and 0.030 Å (ferrous CO) as calculated from inversion of the full positional least-squares matrix. Owing to the atomic resolution, novel features are found in the refined structures. Firstly, two orientations of the haem are observed both in the ferric resting and the ferrous CO states. Secondly, a disordered water molecule bound to the haem iron is found in the ferric resting state. In addition, the accurate structures at atomic resolution enabled the examination of general stereochemical parameters that are commonly used in refinement cycles of protein structures.

1. Introduction

The use of tunable high-intensity well collimated X-rays from synchrotron-radiation sources together with the development of cryotechniques have enabled the improvement of diffraction data quality and, in many cases, attainment of atomic resolution (AR). According to a definition suggested by Sheldrick (1990), AR data should extend to at least 1.2 Å, with 50% or more of the theoretically measurable reflections in the outer range having $I > 2\sigma(I)$. Most of the AR structures are still restricted to small proteins, but some AR structures with molecular weights greater than 40 kDa have been reported (Tame *et al.*, 1996; Tame, 2000; Ermler *et al.*, 1997; Matsumoto *et al.*, 1999; Luan *et al.*, 2000; Foadi *et al.*, 2000). These AR data sets will be useful to examine the applicability of *ab initio* phasing techniques to larger macromolecules, as well as to validate the stereochemical parameters that are used routinely in the refinement cycles of protein structures. The availability of larger protein structures refined to AR will benefit a library of stereochemical target values by adding proteins with different folds with different percentages of secondary-structure elements (EU 3-D Validation Network, 1998). The benefits of AR have been reviewed recently (Longhi *et al.*, 1998; Dauter *et al.*, 1995, 1997).

The nitric oxide reductase cytochrome P450nor (P450nor) from the fungus *Fusarium oxysporum* is a haem enzyme which consists of 403 amino-acid residues (46 kDa), a relatively large protein molecule for structural studies at AR. Since the structure was determined at 2.0 Å resolution at room temperature (Park, Shimizu, Adachi, Nakagawa *et al.* 1997),

efforts have been made to elucidate the catalytic mechanism by which the enzyme reduces NO to N_2O. The X-ray structure of native and mutant P450nor at cryogenic temperature (100 K) and at 1.7 Å resolution revealed that a network of water molecules in a wide cavity near the catalytic site plays a crucial role as a proton-delivery path (Shimizu, Obayashi *et al.*, 2000). During the course of these studies, the crystallization conditions have been refined to enable us to obtain crystals that can provide data sets to 1.00 Å resolution. In addition, intense well collimated short-wavelength X-rays, cryocooling devices and fast-readout CCD detectors have become available at third-generation synchrotron facilities, which allowed us to collect the AR data set using only one crystal. Here, we report the AR structures of the ferric resting and the ferrous carbonmonoxy (CO) forms of P450nor.

2. Materials and methods

2.1. Crystallization and data collection

Crystals of the ferric form were obtained by the sitting-drop vapour-diffusion method using 36% PEG 4000, 0.1 *M* MES, 10% glycerol at pH 7.0 and were improved by the use of microseeding (Park, Shumizu, Adachi, Shiro *et al.*, 1997). Crystals grow in approximately 3 or 4 d to typical dimensions of 0.6 × 0.4 × 0.4 mm. The crystals can be cryocooled directly in the mother liquid without adding cryoprotectant. Some crystals were converted to the CO complex by soaking in CO-saturated mother liquid in the presence of sodium dithionite ($Na_2S_2O_4$). The crystals were flash-frozen in liquid ethane. For data collection, the flash-frozen crystal was transferred to a stream of cold nitrogen gas at 100 K. The diffraction data were collected at the SPring-8 beamline BL44B2 (RIKEN Structural Biology Beamline II) using a MAR CCD 165 detector (Adachi *et al.*, 2002). Relatively short wavelength X-rays (λ = 0.70 Å) were selected in order to record data to 1.0 Å resolution in the detector area of 165 mm diameter and to reduce absorption effects. Two data sets at different resolution ranges (1.0–1.9 and 1.8–10 Å) were collected in order to maximize the coverage of the dynamic range of the intensities. The oscillation angles, ranges and crystal orientation were optimized with *DPS*/*MOSFLM* (Rossmann & van Beek, 1999; Leslie, 1992). All data were indexed and integrated with *DPS*/*MOSFLM* and scaled using programs from the *CCP*4 suite (Collaborative Computational Project, Number 4, 1994).

Data-collection and processing parameters are summarized in Table 1. No significant decay was detected as judged by I/σ over the course of data collection. 1 745 175 and 2 238 315 observations were merged to give 204 021 and 175 256 unique reflections for the ferric resting and the ferrous CO states, respectively. The completeness of the two data sets is more than 90% in the 30.0–1.0 Å range.

Table 1
Summary of data-collection and refinement statistics.

Values in parentheses refer to the highest resolution shell.

	Ferric resting	Ferrous CO
Data collection		
PDB code	1jfb	1jfc
Wavelength (Å)	0.7	0.7
Temperature (K)	100	100
Space group	$P2_12_12_1$	$P2_12_12_1$
Unit-cell parameters (Å)	a = 54.66, b = 82.13, c = 85.84	a = 54.65, b = 82.97, c = 85.62
Resolution range (Å)	100–1.00	100–1.05
No. of observations	1745175	2238315
No. of unique reflections	204021	175256
Completeness (%)	98.1 (96.6)	97.5 (91.3)
R_{merge}† (%)	4.6 (26.2)	6.5 (31.7)
Mean I/σ	7.1 (3.5)	7.0 (2.8)
Solvent content (%)	35	35
α-Helix (%)	53	53
β-Sheet (%)	9	9
Refinement		
Residues	403	403
Molecular mass (kDa)	46	46
Solvent sites		
Full	957	7402
Partial	88	152
Refinement resolution (Å)	10–1.00	10–1.05
Parameters/reflections ($I > 0$)	38979/203704	38397/175082
R factor/R_{free}‡ (%)	10.2/13.9	11.7 / 15.2
wR^2§	25.3	28.7
R.m.s. deviations from ideal geometry		
1–2 bond distances (Å)	0.016	0.015
1–3 bond distances (Å)	0.033	0.031
E.s.d. for all atoms¶ (Å)	0.028	0.030

† $R_{merge} = \sum|I_i - \langle I\rangle|/\sum|I_i|$, where I_i is the intensity of an observation and $\langle I\rangle$ is the mean value for that reflection and the summations are over all reflections. ‡ R factor = $\sum||F_o(h)| - |F_c(h)||/\sum F_o(h)$, where F_o and F_c are the observed and calculated structure-factor amplitudes, respectively. The free R factor was calculated with 5% of the data. § $wR^2 = \{\sum[w(F_o^2 - F_c^2)^2]/\sum[w(F_o^2)^2]\}^{1/2}$. ¶ Estimated standard deviations (e.s.d.s) calculated from inversion of the full positional least-squares matrix.

2.2. Structural refinement

Structural refinements of the ferric resting and the ferrous CO states were carried out using the same procedures. The structure at 1.7 Å resolution (Shimizu, Park *et al.*, 2000) was used as the starting model in each case. Attempts at *ab initio* phasing using *ARP*/*wARP* (Perrakis *et al.*, 1997, 1999) were not successful for either data set. More conventional refinement was therefore used instead. 5% of the reflections were set aside for cross-validation analysis by means of R_{free}. Initial rigid-body refinement was carried out using *X-PLOR* (Brünger, 1992) in the 6.0–2.3 Å resolution range and simulated-annealing protocols were employed. The resolution was increased stepwise from 2.3 to 1.3 Å. After each step, $2F_o - F_c$ and $F_o - F_c$ electron-density maps were calculated and the model was rebuilt if necessary using *TURBO-FRODO* (Roussel & Cambillau, 1989). The refinement of the ferric resting state led to an R factor of 24.2% and an R_{free} of 27.3%. This model contains about 360 water molecules and no multiple conformations were modelled in this step.

This model was further refined using the conjugate-gradient least-squares (CGLS) method with *SHELX*97 (Sheldrick, 1997). The weighting scheme was fixed at 'WGHT 0.1'. SWAT was applied to correct the effect of bulk solvent. After each refinement cycle, the difference Fourier map was analyzed automatically to find solvent sites (the highest peaks at sites

where a water molecule forms no bad contacts and makes at least one geometrically plausible hydrogen bond to a polar atom). The corresponding solvent sites were automatically appended in the output file. After every run, solvent atoms which had either electron density lower than 1.5σ in the $2F_o - F_c$ map and 3σ in the $F_o - F_c$ solvent omit map or B factors of higher than about 60 Å^2 were removed. The shortest distance acceptable for solvent–solvent and solvent–protein pairs of atoms was 2.25 Å and the maximum hydrogen-bond distance was set to 3.3 Å. The porphyrin and CO structures were refined with distance restraints. In this procedure, the resolution was increased stepwise from 1.3 to 1.0 Å. The refinement of the ferrous CO state converged to an R factor of 22.2% and an $R_{\rm free}$ of 25.0%. After this step, anisotropic refinement was carried out with several conjugate-gradient cycles using the maximum resolution. The restraints of the CO ligand and porphyrin were gradually removed and the final CGLS refinement was performed without any restraints. The first round of anisotropic refinement resulted in a sharp fall in the R factor to 16.8% and in the $R_{\rm free}$ to 21.1% (the ferric resting form). After each refinement round, alternative conformations for the side chains and main chains were introduced. The occupancies of the components of each conformation were individually refined and their sum was constrained to unity. Solvent sites in the vicinity of disordered side chains were selected as partially occupied. H atoms were included as riding atoms, lowering the R values by more than 1.0%. In this stage of model building, a glycerol molecule was substituted for water molecules. After 120 CGLS cycles, in which additional solvent molecules and alternative conformations were introduced, anisotropic refinement of 403 protein residues, one porphyrin, one glycerol and approximately 900 water molecules with data in the range 10.0–1.0 Å converged with an R factor of 10.9% and an $R_{\rm free}$ of 14.6% (the ferric resting form). This model was further refined using the block-matrix least-squares calculation in *SHELX*97, where each block consisted of 20–40 residues overlapping by one residue with the adjacent block. At the final stage of the refinement, a full-matrix least-squares calculation was carried out in order to obtain the estimated atomic coordinate errors by matrix inversion. All restraints were switched off for this calculation. The final R factor and $R_{\rm free}$ were 10.2 and 13.9% for 203 704 reflections between 10.0 and 1.00 Å for the ferric resting state and 11.7 and 15.2% for 175 082 reflections between 10.0 and 1.05 Å for the ferrous CO state, respectively. The final statistics for the refined models are listed in Table 2.

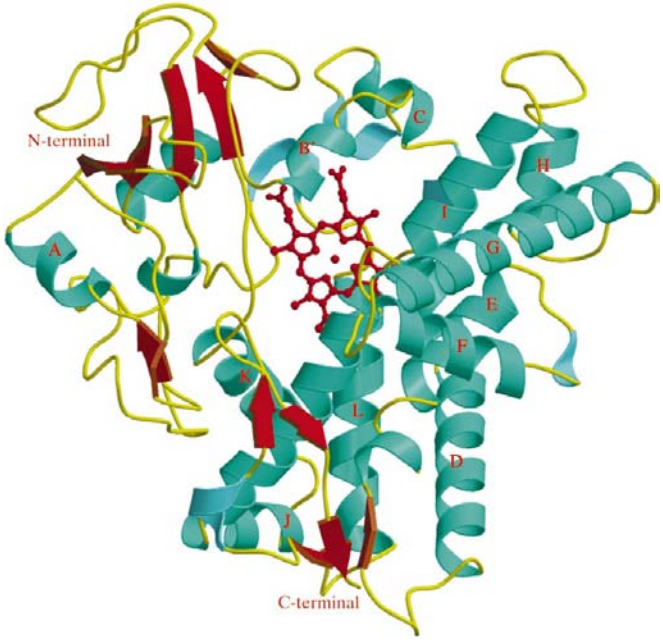

Figure 1
Schematic drawing of overall structure of the P450nor in the ferric resting state: α-helices are shown as green coils and are labelled from A to L, 3_{10}-helices as cyan coils, β-strands as red arrows and loops as yellow tubes. The haem is represented by a ball-and-stick model. This figure was prepared with *MOLSCRIPT* (Kraulis, 1991).

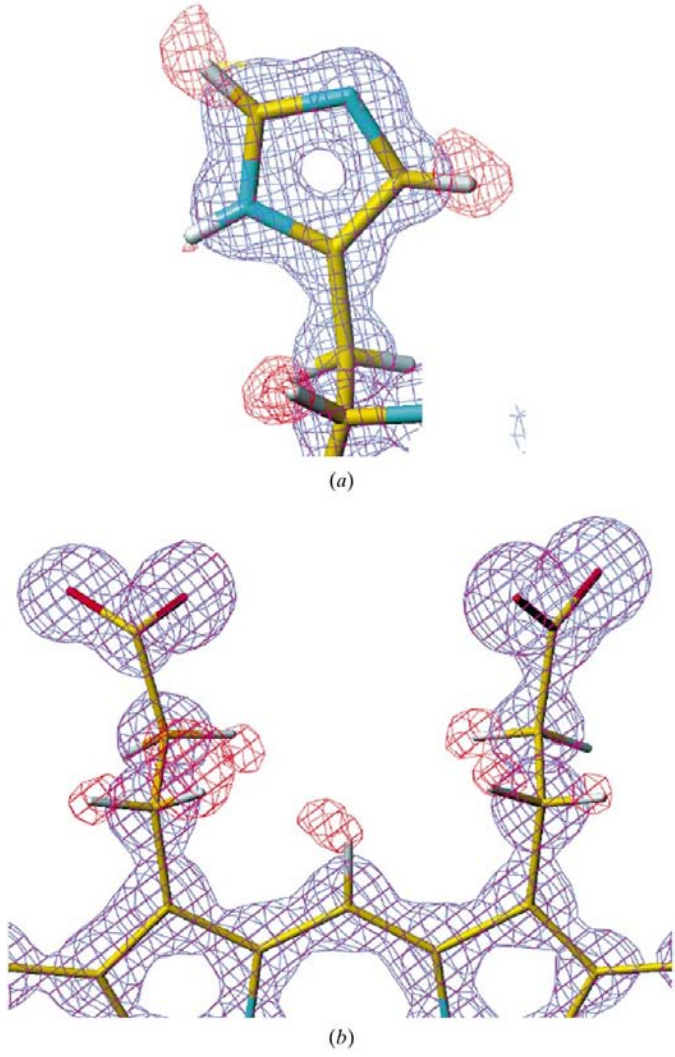

Figure 2
$2F_o - F_c$ map contoured at 1.5σ (blue) and $F_o - F_c$ map contoured at 2.0σ (red) around (*a*) histidine residue and (*b*) haem propionate in an anisotropic model obtained after removal of H atoms followed by three CGLS refinement cycles.

3. Results and discussion

3.1. Overall quality of the electron-density maps

Fig. 1 shows the overall fold of the P450nor. As expected, the quality and the detail of the electron-density map were drastically improved at this resolution compared with the map at 1.7 Å resolution. Fully anisotropic refinement of P450nor resulted in remarkable improvements in the final map. Most of the individual atoms have spherical or ellipsoidal electron densities in the $2F_o - F_c$ map contoured at 3.5σ. The expected conformation of the histidine imidazole ring is confirmed by the visible difference between N and C atoms. The correct conformation of most asparagine and glutamine residues can also be determined directly from the electron density. The refinement with anisotropic thermal parameters against diffraction data to 1.00 and 1.05 Å resolution converged to R factors of 10.2 and 11.7% for the ferric resting and ferrous CO states, respectively. No electron density was seen around the N-terminal four residues in the lower resolution structure of P450nor (Park, Shimizu, Adachi, Nakagawa *et al.*, 1997; Shimizu, Obayashi *et al.*, 2000; Shimizu, Park *et al.*, 2000) and these residues are still not clearly defined in the 1.00 Å structure.

An interesting feature of atomic resolution structures is the ability to deduce the position of H atoms. A difference omit map, in which all H atoms are removed, was computed using refined phases at 1.00 Å. To avoid model bias resulting from over-refinement, three CGLS cycles were performed. As shown in Fig. 2, $F_o - F_c$ peaks at the 2σ level corresponding to the H atoms of a histidine residue and of a methylene group of haem propionate were observed. The final models contain 2385 protein non-H atoms, 3361 and 3379 H atoms and 1045 and 892 water molecules in the ferric resting and the ferrous CO states, respectively.

The coordinate errors of the final models were determined as the estimated standard deviations (e.s.d.s) by inversion of the full-matrix least-squares matrix after removal of all restraints. The mean e.s.d.s for all atoms are 0.028 and 0.030 Å for ferric resting and ferrous CO states, respectively. The e.s.d.s averaged over main-chain atoms of each residue are plotted as a function of the residue numbers for the ferric resting and the ferrous CO states (Fig. 3). The e.s.d.s in both structures are as low as 0.02 Å, except for several sites in B' helix and loop regions. Since these residues are located at the most flexible parts of the structure, they have high B factors and weak electron densities. As expected, e.s.d.s strongly correlate with the corresponding B factors.

3.2. Haem orientation and geometry

The $2F_o - F_c$ electron-density map (1.5σ) and the $F_o - F_c$ map (3σ) of the haem in the ferric resting and the ferrous CO states are superimposed on the model structure in Fig. 4. If we assume one orientation of the haem (the major form), $F_o - F_c$ peaks are clearly observed at the 1- and 3-methyl positions. These peaks show the existence of another orientation of the haem (the minor form) in the crystal, which is rotated by a 180° rotation around the α,γ-*meso* axis. This type of double orientation of the haem in the crystal structure has never been observed in normal haem proteins or enzymes such as myoglobin (Mb), haemoglobin (Hb) or other P450s; only one case has been reported in the haem-bound haemophore (haem transporter) HasA (Arnoux *et al.*, 2000). However, the flipped orientation of the haem has been frequently reported in solution structures of haem proteins by CD (Aojula *et al.*, 1986) and NMR studies (La Mar *et al.*, 1983), indicating that the two interconverting protein forms are present at equilibrium. Thus, it is most probable that the two orientations are nearly equally stable in P450nor, so that both forms are crystallized in a single crystal. The occupancies of the reversed orientation of the haem (the minor form) refine to 38.3 and 39.1% for the ferric resting and the ferrous CO states, respectively.

Functional differences between the two forms possessing the different haem orientation have been examined in some haem proteins; sperm whale myoglobin exhibits identical O_2- and CO-binding properties (Light *et al.*, 1987), while monomeric insect Hb displays a difference in the Bohr effect (Gersonde *et al.*, 1986) and cytochrome b_5 shows a difference of ~30 mV in the redox potential (Walker *et al.*, 1988). In the case of P450nor, the functional properties measured so far (binding rates of CO and NO, redox potential and catalytic rate constants of NO reduction) are monophasic and functional differences between the two forms with different haem orientations are apparently negligible.

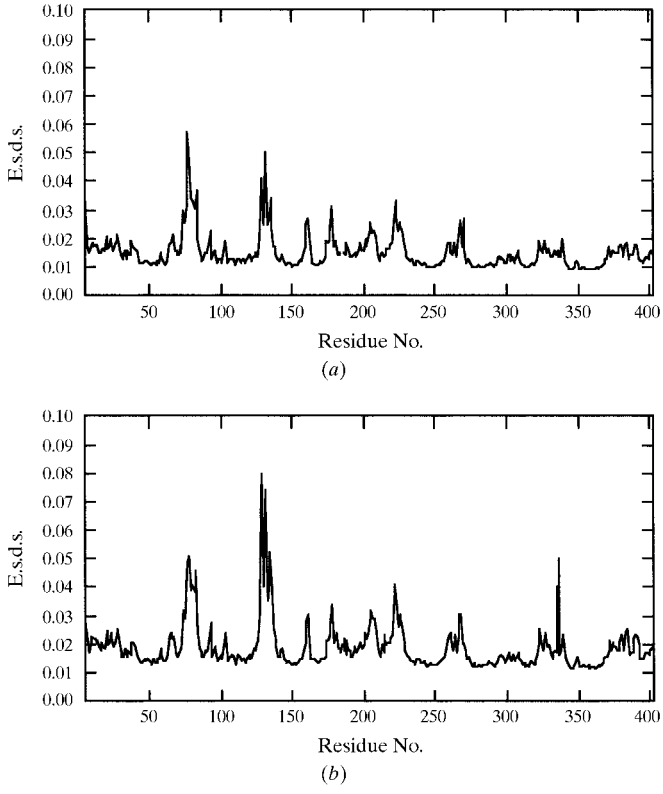

Figure 3
Plot of the main-chain estimated standard deviations (e.s.d.s) for each residue of (*a*) the ferric resting state and (*b*) the ferrous CO state calculated from inversion of the full positional least-squares matrix.

Table 2
Comparison of the expected values for stereochemical parameters with the actual values observed in three P450nor structures.

	Original parameters		Ferric resting (1.00 Å)		Ferrous CO (1.05 Å)		Ferric resting (1.7 Å)†	
	Mean	s.d.‡	Mean	s.d.‡	Mean	s.d.‡	Mean	s.d.‡
χ_1 dihedral angle (°)								
gauche(−)	64.1	15.7	64.1	9. 6	64.0	7.2	59.2	13.0
trans	183.6	16.8	181.2	9.8	183.0	12.2	180.0	11.7
gauche(+)	−66.7	15.0	−66.1	9.0	−66.2	8.2	−68.6	13.8
χ_2 dihedral angle (°)	177.4	18.5	174.6	11.3	174.5	11.0	177.7	15.2
Proline (φ) torsion angle (°)	−65.4	11.2	−66.7	10.9	−66.5	10.8	−65.9	13.3
Helix (φ) torsion angle (°)	−65.3	11.9	−65.4	11.2	−65.2	11.2	−65.2	10.4
Helix (ψ) torsion angle (°)	−39.4	11.3	−39.9	9.7	−40.0	9.9	−39.9	9.7
ω dihedral angle (°)	179.6	4.7	179.7	5.7	179.9	5.8	180	1.1
CA chirality ζ (CA−N−C−CB) (°)	33.9	3.5	34.0	1.9	34.0	1.9	34.8	0.9
Hydrogen-bond energies (kcal mol^{-1})§	−2.0	0.8	−2.1	0.6	−2.1	0.6	−2.0	0.7
Residues in most favoured region (%)	>90		92.6		92.8		90.5	

† Shimizu, Park *et al.* (2000). ‡ Standard deviation. § 1 kcal mol^{-1} = 4.184 kJ mol^{-1}.

The Fe-ligand geometry of P450nor, other haemoproteins and model compounds are summarized in Table 3. The haem and ligand geometries of the new structure differ substantially from those of previous crystal structures (Park, Shimizu, Adachi, Nakagawa *et al.*, 1997; Shimizu, Obayashi *et al.*, 2000) which were refined at lower resolution with stereochemical restraints and did not include uncertainty estimates. The e.s.d.s for the porphyrin atoms of the new models show high accuracy, with averages of 0.010 and 0.014 Å in the ferric and the ferrous states, respectively.

The structure of the ferrous CO state showed clear electron density around the fully occupied Fe-bound CO (Fig. 5*a*). Fig. 6 shows the haem–CO complex in P450nor. Displacement ellipsoids are drawn at the 40% probability level and only the orientation of the haem in the major form is shown. The Fe—C—O coordination geometry is nearly linear, with a bending angle of 172.2 ± 1.79°, and is tilted by an angle of 5.7° from the normal to the haem plane. The carbonyl O atom of Gly239 is located at a short distance from the CO O atom (2.87 Å) and sterically pushes the CO molecule toward the porphyrin *β-meso* direction, resulting in the slightly bent Fe—C—O bond. The Fe—CO and C—O distances are 1.82 ± 0.016 and 1.16 ± 0.016 Å, respectively. Upon CO binding to the haem, the displacement of the Fe atom from the haem plane reduces from 0.18 to 0.06 Å, resulting in an in-plane configuration. The Fe—S (Cys352) bond length in the ferrous CO state (2.33 ± 0.003 Å) is slightly shorter than that in the ferric resting state (2.39 ± 0.004 Å).

The bond angles obtained from our X-ray analysis can be compared with those of the model compounds Mb and P450cam (Table 3*b*). Studies of model compounds such as Fe(TPP)(py)(CO) have shown that CO prefers a linear geometry in the absence of steric hindrance, in order to maximize Fe $d\pi$—CO π^* back-bonding (Peng & Ibers, 1976; Caron *et al.*, 1979). Previously reported crystal structures of CO complex of Mb have shown disordered and bent CO conformations (120–140°), which were explained in terms of the interactions between ligand and the distal His residue (Kuriyan *et al.*, 1986). However, recent results from crystallographic studies of the myoglobin–CO complex at atomic resolution suggested a nearly linear conformation with a bending angle of 171–173° and a tilt angle of 4.8–9.0° (Vojtěchovský *et al.*, 1999; Kachalova *et al.*, 1999).

In contrast, the bound CO in P450cam is bent and tilted by 14° from the haem normal owing to a steric effect of the substrate (Raag & Poulos, 1989). The Fe—CO distance of P450cam was found to be 2.04 Å, slightly longer than that of P450nor (1.82 ± 0.015 Å). The C—O distance in P450nor (1.16 Å) is close to that in P450cam (1.12 Å). Our resonance Raman data showed that the Fe-ligand stretching frequency for the ferrous CO state was located 4 cm^{-1} higher in P450nor than in camphor-bound P450cam (Shiro *et al.*, 1994). In addition, our infrared (IR) spectroscopic study showed that stretching mode of the C—O in P450nor (1942 cm^{-1}) is at almost the same position as that in P450cam (1940 cm^{-1}) (Shiro *et al.*, 1997). These observations indicate that the back-donation from the iron *d* orbital to the ligand π^* orbital is the same in magnitude in P450nor and P450cam. Thus, σ donation from the CO $2\pi\sigma$ orbital to the iron $3d\sigma$ orbital is increased, giving a stronger Fe—CO bond in P450nor than in P450cam.

3.3. Water and glycerol molecules

As expected, the number of visible solvent molecules increased upon extension of the diffraction data to atomic resolution (Table 1). The majority of the partially occupied waters are located close to the disordered residues and have a connection with one of the alternative side-chain conformations. Part of the solvent structure is organized in pentagonal or hexagonal rings which are located in the distal haem pocket and between the neighbouring protein molecules.

In the ferric resting form, an elongated electron density corresponding to an Fe-bound water molecule is observed (Fig. 5*b*). This water molecule was not observed in the crystal structure at room temperature, probably owing to its high temperature factor. The water molecule was treated as disordered and the occupancies are estimated as 0.55 (close to the iron) and 0.45 (distant from the iron). The powder EPR spectrum of the ferric resting state of the P450nor crystal was measured and was characteristic of a ferric low-spin species with a small amount of ferric high-spin species (Park, Shimizu, Adachi, Shiro *et al.*, 1997). The existence of two binding modes for the water molecule might be related to the mixture of spin states in the haem iron of the ferric resting state. Weak binding of the haem pocket water molecule to the haem iron may be

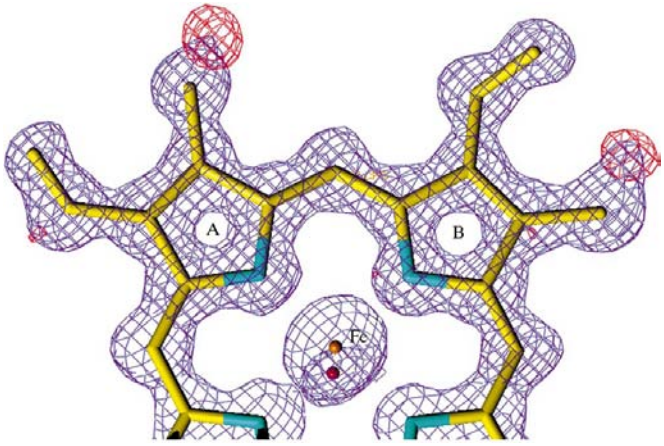

Figure 4
Electron density corresponding to two orientations of the haem. The $2F_o - F_c$ map (blue) is contoured at 2σ and the $F_o - F_c$ map (red) is contoured at 3σ. The thin line model presents one of two orientations of the haem.

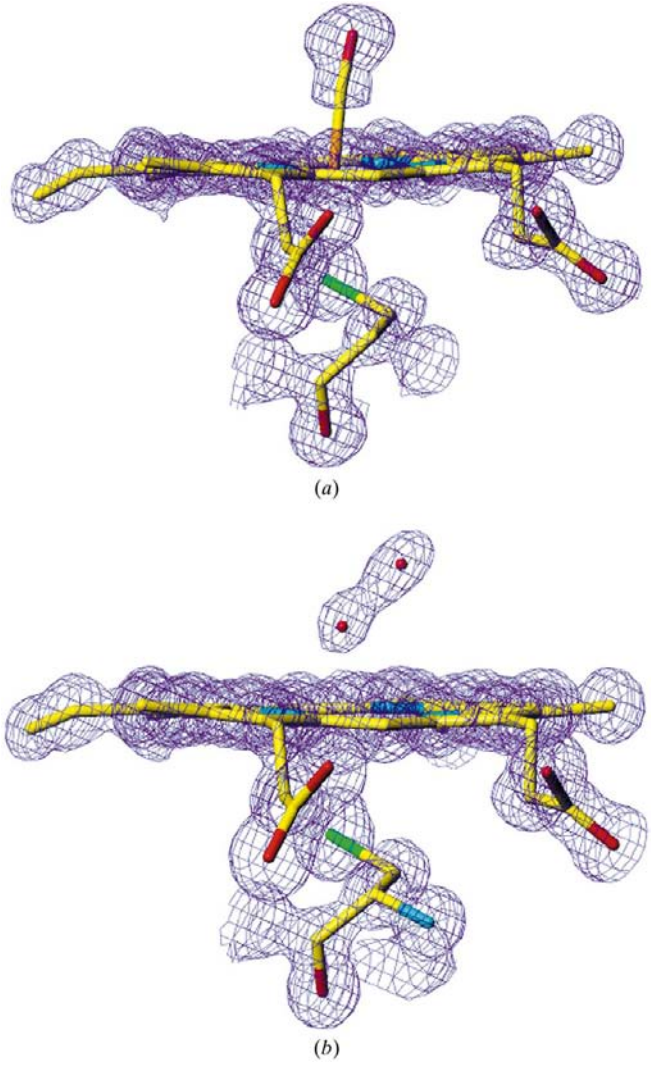

Figure 5
Final $2F_o - F_c$ electron density (1.5σ) of the haem and its axial ligand: (*a*) ferrous CO state, (*b*) ferric resting state.

functionally important, as the NO molecule must bind the haem very rapidly to achieve the extraordinary high turnover rate of the enzyme (Shiro *et al.*, 1995).

Electron density corresponding to a glycerol molecule (contained in the solution of protein preparation) was observed on the surface at the proximal side. The electron densities of C and O atoms in glycerol can be distinguished based on the volume of the density contoured at 1.5σ. These electron densities were assigned as water molecules in the previous 1.7 Å structures at cryotemperature (Shimizu, Obayashi *et al.*, 2000). The glycerol molecule is fully occupied and has a low temperature factor. The glycerol molecule interacts with the side chains of the proximal residues (Asp90, His350 and Arg292).

3.4. Structural validation and conformational properties of the AR structures

The atomic resolution structures of the ferric resting and the ferrous CO states were validated by *PROCHECK* (Laskowski *et al.*, 1993) (Table 2). The Ramachandran plot shows a higher percentage (ferric resting state, 92.6%; ferrous CO state, 92.8%) of residues in the most favoured regions than that of 1.7 Å structure (90.5%); no residues were found in the disallowed or generously allowed regions. Analysis of the stereochemistry of the atomic resolution structure shows that

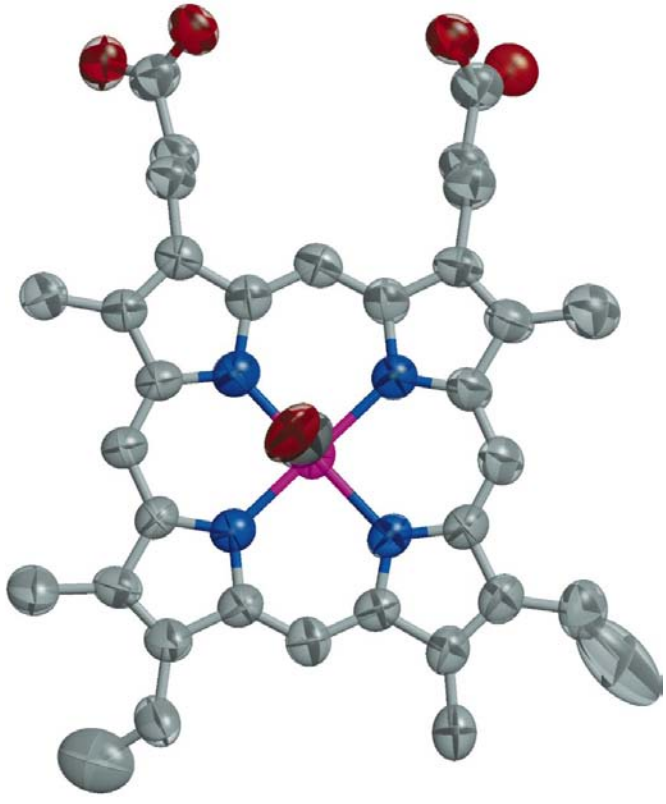

Figure 6
The haem–CO complex in P450nor (ferrous CO form). Displacement ellipsoids are drawn at the 40% probability level and only the orientation of the haem in the major form is shown.

Table 3
Comparison of haem geometry and CO bend and tilt angles in P450nor, P450cam, Mb and model compounds.

(*a*) Haem geometry.

	P450nor	P450nor CO	P450cam CO†	Fe(TPP)(py)(CO)‡
Refinement	*SHELX*97	*SHELX*97	*PROFFT*	
Resolution (Å)	1.00	1.05	1.9	
Fe—CO/H_2O (Å)	2.03 ± 0.0138	1.82 ± 0.0155	2.04	1.77
C—O (Å)	—	1.16 ± 0.0158	1.12	1.12
Fe—Npor plane (Å)	0.18	0.06	−0.02	0.02
Fe—S (Å)	2.33 ± 0.0032	2.39 ± 0.0038	2.41	

(*b*) CO bend and tilt angles.

	P450nor	P450cam†	Mb§	Mb¶	Fe(TPP)(py)(CO)‡
Resolution (Å)	1.05	1.9	1.15	1.2	
Bend angle (°)	172.2 ± 1.79	166.0	172.6 ± 1.9	171.0 ± 3	179
Tilt angle (°)	5.7	4.7	4.8	9.0	0.0

† Raag & Poulos (1989). ‡ Peng & Ibers (1976). § Kachalova *et al.* (1999). ¶ Vojtěchovský *et al.* (1999).

all geometric parameters are within the limits expected for this resolution. The mean deviation from the ideal geometry of the atomic resolution structure is larger than that present in the final refinement statistics of the 1.7 Å structure because of the looser restraints on the stereochemistry.

The statistics of the bond distances and bond angles for the polypeptide backbone and C^{β} atoms are given in Table 2. The majority of the various types of bond distances and bond angles follow the normal distribution. However, for ω and χ angles statistically significant discrepancies from original parameters have been found. Such discrepancies from the ideal geometries have been systematically validated using several atomic resolution structures and validation tools (EU 3-D Validation Network, 1998).

The ω torsion angles have a mean value of 179.8° with a standard deviation of 5.8° (Fig. 7*a*). ω varies from 193.9° (Thr104) to 166.6° (Met89), showing that the peptide bond is not quite planar and has a slightly asymmetric distribution. The electron density of these regions also confirms the validity of the non-planar conformation. The distribution seems to reflect a general property of proteins.

The values of the χ_1 (N—C^{α}—C^{β}—X^{γ}, where X corresponds to C, S or O atoms depending on the residue type) and χ_2 (C^{α}—C^{β}—X^{γ}—X^{δ}) torsion angles show similar distributions to those expected on the basis of simple energy calculations; certain combinations of χ_1 and χ_2 are preferred (Ponder & Richards, 1987). Overall analysis showed the torsion angles are tightly clustered about three possible rotameric states (*gauche*−, *gauche*+ and *trans*) (Fig. 7*b*). Omitting proline, the mean values and standard deviations of the atomic resolution structures are 64.1 (9.6), 181.2 (9.8), −66.1° (9.0°) when residues with multiple conformations are included and 64.0 (9.9), 180.5 (9.9), −65.8° (8.8°) when they are excluded. This is a narrower distribution than found in the 1.7 Å structure [59.2 (13.0), 180.0 (11.7), −68.6° (13.8°)] (Table 2*a*). In the ferric resting state model, uncommon conformations are found only for Lys77 (227°) and Met333 (99.3°): Lys77 belongs to the B' helix, which is located on the surface of the molecule, and Met333 has a discretely disordered side chain.

3.5. Amino-acid residues with alternate conformations

Electron-density maps calculated after the anisotropic refinement clearly showed that about 10% of residues have multiple conformations. In the isotropic refinement stage, the

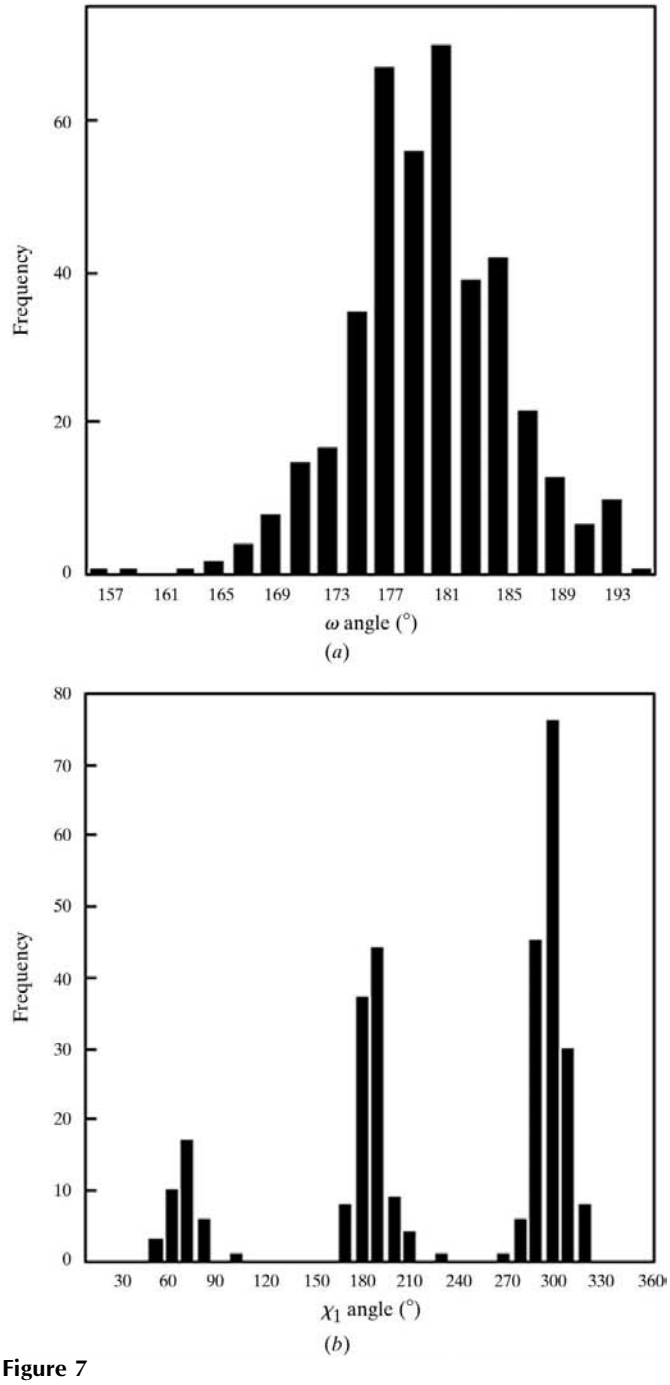

Figure 7
Histograms of torsion angles for ferric resting states: (*a*) ω angle, (*b*) χ_1 angle.

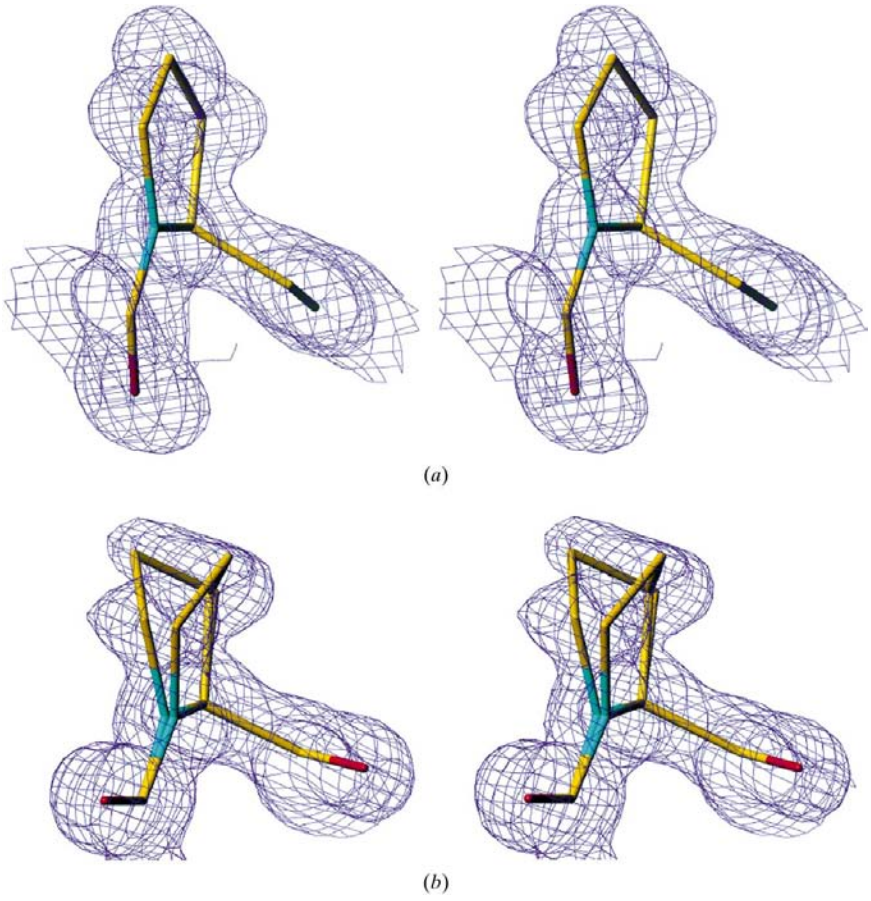

Figure 8
Stereoview of the $2F_o - F_c$ map around Pro9 is contoured at 1.5σ: (*a*) ferrous CO state, (*b*) ferric resting state.

electron densities of disordered side chains were observed in only five residues. A further 24 residues were found to be disordered in the early stage of anisotropic refinement. Introduction of disordered segments followed by rebuilding of the side chain and water molecules improved detail in the electron-density maps and provided more accurate delineation of the effects of conformational disorder and partial occupancy. Most of the disordered residues are located at the surface of the protein, but a few completely buried side chains residues such as serine, valine and threonine were also assigned multiple conformations. Finally, 40 and 42 residues were modelled as two conformations in the ferric resting and the ferrous CO states, respectively. The side chain of Ser185 consists of three conformers in both structures.

The displacement of the C^{γ} atoms of Pro residues in P450nor was computed using *WHATCHECK* (Hooft *et al.*, 1996). Most of proline rings have a puckering amplitude Q of between 0.20 and 0.45 Å, which gives the r.m.s. out-of-plane deviation of the five ring atoms. However, two residues [Pro269 (Q = 0.03) and Pro339 (Q = 0.13)] in the ferric resting state and three residues [Pro9 (Q = 0.17), Pro269 (Q = 0.09) and Pro339 (Q = 0.01)] in the ferrous CO state are outside the expected range. The electron densities at these residues show only slightly puckered proline rings. The positions of these residues are identical in both the ferric and ferrous states, except for Pro9 which forms double-puckered conformations in the ferric state (Fig. 8).

4. Concluding remarks

Cytochrome P450nor has been refined anisotropically to a resolution of 1.00 and 1.05 Å in the ferric and the ferrous carbonmonoxy states, respectively. The refinement led to significant improvement in the accuracy of the model compared with the best structure to date (1.7 Å). P450nor consists of 403 amino-acid residues (46 kDa) and is one of the largest proteins refined to atomic resolution thus far. Owing to the improvement in resolution, unique features are found in the refined structures. Firstly, two orientations of the haem are significantly populated in both ferric resting and ferrous CO states. The occupancies of the minor form are refined to 38.3 and 39.1% for the ferric resting and the ferrous CO states, respectively. So far, there is no indication that the two forms are biologically different. Secondly, a disordered water is found weakly bound to the haem iron in the ferric resting state. It is possible the protein must weaken the binding of water to the ferric haem in order to promote rapid NO binding. The structures show no movements which explain the reaction pathway. Atomic resolution studies of NO-bound P450nor are needed to understand the NO-reduction mechanism of the enzyme.

We thank T. Iizuka and H. Shoun for helpful discussions. We also thank J. Tame for careful reading of the manuscript. This work was supported in part by grants from the Structural Biology and the MR Science Program in RIKEN (to YS).

References

Adachi, S., Oguchi, T., Tanida, H., Park, S.-Y., Shimizu, H., Miyatake, H., Kamiya, N., Shiro, Y., Inoue, Y., Ueki, T. & Iizuka, T. (2002). In the press.
Aojula, H. S., Wilson, M. T. & Drake, A. (1986). *Biochem. J.* **237**, 613–616.
Arnoux, P., Haser, R., Izadi-Pruneyre, N., Lecroisey, A. & Czjzek, M. (2000). *Proteins Struct. Funct. Genet.* **41**, 202–210.
Brünger, A. T. (1992). *X-PLOR. Version 3.1. A System for X-ray Crystallography and NMR.* Yale University, Connecticut, USA.
Caron, C., Mitschler, A., Riviere, G., Ricard, L., Schappacher, M. & Weiss, R. (1979). *J. Am. Chem. Soc.* **101**, 7401–7402.
Collaborative Computational Project, Number 4 (1994). *Acta Cryst.* D**50**, 760–763.
Dauter, Z., Lamzin, V. S. & Wilson, K. S. (1995). *Curr. Opin. Struct. Biol.* **5**, 784–790.
Dauter, Z., Lamzin, V. S. & Wilson, K. S. (1997). *Curr. Opin. Struct. Biol.* **7**, 681–688.

Ermler, U., Grabarse, W., Shima, S., Goubeaud, M. & Thauer, R. K. (1997). *Science*, **278**, 1457–1462.
EU 3-D Validation Network (1998). *J. Mol. Biol.* **276**, 417–436.
Foadi, J., Woolfson, M. M., Dodson, E. J., Wilson, K. S., Jia-xing, Y. & Chao-de, Z. (2000). *Acta Cryst.* D**56**, 1137–1147.
Gersonde, K., Sick, H., Overkamp, M., Smith, K. M. & Parish, D. W. (1986). *Eur. J. Biochem.* **157**, 393–404.
Hooft, R. W. W., Vriend, G., Sander, C. & Abola, E. E. (1996). *Nature (London)*, **381**, 272.
Kachalova, G. S., Popov, A. N. & Bartunik, H. D. (1999). *Science*, **284**, 473–476.
Kraulis, P. (1991). *J. Appl. Cryst.* **24**, 946–950.
Kuriyan, J., Wilz, S., Karplus, M. & Petsko, G. A. (1986). *J. Mol. Biol.* **192**, 133–154.
La Mar, G. N., Davis, N. L., Parish, D. W. & Smith, K. M. (1983). *J. Mol. Biol.* **168**, 887–896.
Laskowski, R. A., MacArthur, M. W., Moss, D. S. & Thornton, J. M. (1993). *J. Appl. Cryst.* **26**, 283–291.
Leslie, A. G. W. (1992). *Jnt CCP4/ESF–EAMCB Newsl. Protein Crystallogr.* **26**.
Light, W. R., Rohlfs, R. J., Palmer, G. & Olson, J. S. (1987). *J. Biol. Chem.* **262**, 46–52.
Longhi, S., Czjzek, M. & Cambillau, C. (1998). *Curr. Opin. Struct. Biol.* **8**, 730–738.
Luan, P., Heine, A., Zeng, K., Moyer, B., Greasely, S. E., Kuhn, P., Balch, W. E. & Wilson, I. A. (2000). *Traffic*, **1**, 270–281.
Matsumoto, T., Nonaka, T., Hashimoto, T., Watanabe, T. & Mitsui, Y. (1999). *Proc. Jpn Acad.* **75**, 269–274.
Park, S.-Y., Shimizu, H., Adachi, S., Nakagawa, A., Tanaka, I., Nakahara, K., Shoun, H., Nakamura, H., Iizuka, T. & Shiro, Y. (1997). *Nature Struct. Biol.* **4**, 827–832.
Park, S.-Y., Shimizu, H., Adachi, S., Shiro, Y., Iizuka, T., Nakagawa, A., Tanaka, I., Shoun, H. & Hori, H. (1997). *FEBS Lett.* **412**, 346–350.
Peng, S.-M. & Ibers, J. A. (1976). *J. Am. Chem. Soc.* **98**, 8032–8036.
Perrakis, A., Morris, R. J. & Lamzin, V. S. (1999). *Nature Struct. Biol.* **6**, 458–463.
Perrakis, A., Sixma, T. A., Wilson, K. S. & Lamzin, V. S. (1997). *Acta Cryst.* D**53**, 448–455.
Ponder, J. W. & Richards, F. M. (1987). *J. Mol. Biol.* **193**, 775–791.
Raag, R. & Poulos, T. L. (1989). *Biochemistry*, **28**, 7586–7592.
Rossmann, M. G. & van Beek, C. G. (1999). *Acta Cryst.* D**55**, 1631–1653.
Roussel, A. & Cambillau, C. (1989). *Silicon Graphics Geometry Partner Directory*, edited by Silicon Graphics, pp. 77–78. Mountain View, CA: Silicon Graphics.
Sheldrick, G. M. (1990). *Acta Cryst.* A**46**, 467–473.
Sheldrick, G. M. (1997). *The SHELX97 Manual.* University of Göttingen, Germany.
Shimizu, H., Obayashi, E., Gomi, H., Arakawa, H., Park, S.-Y., Nakamura, H., Adachi, S., Shoun, H. & Shiro, Y. (2000). *J. Biol. Chem.* **275**, 4816–4826.
Shimizu, H., Park, S.-Y., Lee, D.-S, Shoun, H. & Shiro, Y. (2000). *J. Inorg. Biochem.* **81**, 191–205.
Shiro, Y., Fujii, M., Iizuka, T., Adachi, S., Tsukamoto, K., Nakahara, K. & Shoun, H. (1995). *J. Biol. Chem.* **270**, 1617–1623.
Shiro, Y., Kato, M., Iizuka, T., Nakahara, K. & Shoun, H. (1994). *Biochemistry*, **33**, 8673–8677.
Shiro, Y., Tsukamoto, K., Obayashi, E., Adachi, S., Iizuka, T., Nomura, M. & Shoun, H. (1997). *J. Phys. IV France*, **7**, 587–591.
Tame, J. R. H. (2000). *Acta Cryst.* D**56**, 1554–1559.
Tame, J. R. H., Sleigh, S. H., Wilkinson, A. J. & Ladbury, J. E. (1996). *Nature Struct. Biol.* **3**, 998–1001.
Vojtěchovský, J., Chu, K., Brendzen, J., Sweet, R. M. & Schlichting, I. (1999). *Biophys. J.* **77**, 2153–2174.
Walker, F. A., Emrich, D., Rivera, J. E., Hanquet, B. J. & Buttlaire, D. H. (1988). *J. Am. Chem. Soc.* **110**, 6234–6240.